THE JOURNAL OF BIOLOGICAL CHEMISTRY VOL. 287, NO. 44, pp. 37371–37382, October 26, 2012
Published in the U.S.A.

Structure of a Proteasome Pba1-Pba2 Complex

IMPLICATIONS FOR PROTEASOME ASSEMBLY, ACTIVATION, AND BIOLOGICAL FUNCTION[*S]

Received for publication, March 27, 2012, and in revised form, July 16, 2012 Published, JBC Papers in Press, August 28, 2012, DOI 10.1074/jbc.M112.367003

Beth M. Stadtmueller[‡1,2], **Erik Kish-Trier**[‡1,3], **Katherine Ferrell**[‡], **Charisse N. Petersen**[‡], **Howard Robinson**[§], **David G. Myszka**[‡], **Debra M. Eckert**[‡], **Tim Formosa**[‡], **and Christopher P. Hill**[‡4]

From the [‡]*Department of Biochemistry, University of Utah School of Medicine, Salt Lake City, Utah 84112-5650 and* [§]*Department of Biology, Brookhaven National Laboratory, Upton, New York 11973-5000*

Background: Pba1-Pba2 facilitates proteasome α-ring assembly.
Results: Pba1-Pba2 binds mature proteasomes using C-terminal motifs and sequesters α-subunit N termini. It does not activate and is not degraded by isolated 20S proteasomes.
Conclusion: Pba1-Pba2 is important for proteasome-dependent maintenance of mitochondrial function. The structure is consistent with multiple roles in proteasome assembly.
Significance: Models of proteasome assembly and Pba1-Pba2 proteasome function are advanced.

The 20S proteasome is an essential, 28-subunit protease that sequesters proteolytic sites within a central chamber, thereby repressing substrate degradation until proteasome activators open the entrance/exit gate. Two established activators, Blm10 and PAN/19S, induce gate opening by binding to the pockets between proteasome α-subunits using C-terminal HbY*X* (hydrophobic-tyrosine-any residue) motifs. Equivalent HbY*X* motifs have been identified in Pba1 and Pba2, which function in proteasome assembly. Here, we demonstrate that Pba1-Pba2 proteins form a stable heterodimer that utilizes its HbY*X* motifs to bind mature 20S proteasomes *in vitro* and that the Pba1-Pba2 HbY*X* motifs are important for a physiological function of proteasomes, the maintenance of mitochondrial function. Other factors that contribute to proteasome assembly or function also act in the maintenance of mitochondrial function and display complex genetic interactions with one another, possibly revealing an unexpected pathway of mitochondrial regulation involving the Pba1-Pba2 proteasome interaction. Our determination of a proteasome Pba1-Pba2 crystal structure reveals a Pba1 HbY*X* interaction that is superimposable with those of known activators, a Pba2 HbY*X* interaction that is different from those reported previously, and a gate structure that is disrupted but not sufficiently open to allow entry of even small peptides. These findings extend understanding of proteasome interactions with HbY*X* motifs and suggest multiple roles for Pba1-Pba2 interactions throughout proteasome assembly and function.

The eukaryotic 20S proteasome (core particle) is a large (~730 kDa) 28-subunit complex that functions as the primary protease of the cytosol and nucleus, where it plays essential roles in numerous homeostatic and regulatory processes (1). The proteasome adopts a barrel-shaped structure that is highly conserved between yeasts and mammals and comprises four stacked heptameric rings, with two α-type end rings and two central β-type rings. Seven related but unique α-subunits (α1–7) and seven related but unique β-subunits (β1–7) each occupy specific locations within their respective rings.

Proteasome assembly follows an ordered, chaperone-assisted process that avoids off-pathway intermediates and aberrant proteolysis and is largely conserved throughout eukaryotes (2). Formation of an α-ring is followed by sequential addition of β-subunits to form half-proteasomes, which dimerize and undergo autocatalytic processing to form mature proteasomes. Three chaperone complexes facilitate assembly, including Ump1 (3), Pba3-Pba4 (4, 5), and the focus of this study, Pba1-Pba2/Poc1-Poc2/PAC1-PAC2 (6–8). Deletion of *PBA1-PBA2* elicits little phenotype in *Saccharomyces cerevisiae* in the absence of other mutations (7, 8), although knock-out of PAC1 causes embryonic lethality in mice (9), and major defects in proteasome assembly are apparent upon knockdown in cultured human cells (6). The leading model is that Pba1-Pba2 binds to the apical side of α-subunit rings in essentially all assembly intermediates and is degraded upon formation of mature 20S proteasomes. Principal roles are thought to include stabilizing the nascent α-ring and blocking off-pathway associations.

The active sites of mature proteasomes are formed at the N termini of the β1, β2, and β5 subunits and are sequestered in the central catalytic chamber, which substrates access through a pore in the center of the α-ring that, by default, is sealed by a gate comprised of the α-subunit N-terminal residues. This repressed conformation is released through interactions with proteasome activators, which are protein factors that bind to the α-rings and open the gate (10). Three distinct activator classes have been identified in eukaryotes, namely the ATP-

* This work was supported by National Institutes of Health Grant RO1 GM59135 (to C. P. H.).
[S] This article contains supplemental Tables S1 and S2, Figs. S1–S4, and additional references.
The atomic coordinates and structure factors (code 4G4S) have been deposited in the Protein Data Bank (http://wwpdb.org/).
[1] Both authors contributed equally to this work.
[2] Present address: Division of Biology, California Institute of Technology, Pasadena, CA 91125-0002.
[3] Supported by Postdoctoral Fellowship National Institutes of Health T32CA092347 Multidisciplinary Cancer Research Training Program (MCRTP).
[4] To whom correspondence should be addressed: Dept. of Biochemistry, University of Utah, Salt Lake City, UT 84112-5650. Fax: 801-581-7959; E-mail: chris@biochem.utah.edu.

independent 11S/PA28/PA26 and Blm10/PA200 activators, and the ATP-dependent 19S/PA700/RP activators. Whereas the proposed physiological roles and overall structures of these activators are highly divergent, they employ some common mechanisms, with binding mediated by C-terminal residues inserting into pockets between proteasome α-subunits, and gate opening triggered by repositioning the Pro-17 reverse turn of proteasome α-subunits.

Notably, three of the six 19S ATPase subunits (as well as their archaeal homolog PAN) and Blm10 display a conserved C-terminal hydrophobic tyrosine-any residue (Hb*YX*)[5] tripeptide that is implicated in both binding and gate opening (11–14). This motivated us to search for other proteins displaying similar C-terminal residues that might bind proteasomes and possibly induce gate opening. One attractive candidate is Pba1-Pba2, which contains Hb*YX* motifs at the C termini of both Pba1 (LYI) and Pba2 (LYN) (*S. cerevisiae* sequences) (15).

Here, we report that Pba1-Pba2 is a stable heterodimer that binds the mature 20S proteasome in an Hb*YX*-dependent manner and that these interactions function in a novel proteasome-related pathway that is important for the maintenance of mitochondrial function. We also report a Pba1-Pba2 proteasome crystal structure that suggests multiple roles in proteasome assembly, thereby explaining why Pba1-Pba2 is associated with α-subunits from the earliest assembly intermediates and also binds the mature proteasome. The structure reveals surprisingly varied Hb*YX* interactions with proteasomes, and our biochemical data argue against the suggestion that the C-terminal Hb*YX* motifs target Pba1-Pba2 for degradation by the 20S proteasome.

EXPERIMENTAL PROCEDURES

Protein Purification—Pba1 (Uniprot no. Q05778) and Pba2 (Uniprot no. P36040; tagged with His_6 and linker SQDP) were co-expressed from a pRSF-Duet vector (Novagen) in BL21(DE3) codon+ (RIL) *Escherichia coli* cells (Stratagene) in auto-induction medium, ZYP-5052 (16) at 37 °C for 6 h, then transferred to 19 °C for 20 h. Mutations were introduced using the QuikChange procedure (Stratagene). Purification was performed at 4 °C. Cell pellets were resuspended and sonicated in lysis buffer containing 25 mM Tris-HCl, pH 7.5, 300 mM NaCl, 2 mM 2-mercaptoethanol, 10 mM imidazole, and protease inhibitors (Sigma), and centrifuged at 20,000 × *g* for 45 min. Clarified lysate was bound to nickel-nitrilotriacetic acid resin (Qiagen), washed in lysis buffer supplemented with 30 mM imidazole, and eluted with an equivalent buffer containing 100 mM NaCl and 500 mM imidazole. Eluted protein was loaded onto a 5-ml HiTrap Q HP column attached to an ÅKTA FPLC (GE Healthcare), washed with buffer A (25 mM Tris-HCl, pH 7.5, 100 mM NaCl, 1 mM DTT), and eluted with a linear gradient of buffer A made up with 1 M NaCl. Fractions containing Pba1-Pba2 were identified by SDS-PAGE, concentrated by ultrafiltration, and passed over a Superdex-200 16/60 size exclusion column (GE Healthcare) in 25 mM Tris-HCl, pH 7.5, 100 mM NaCl, and 1 mM DTT. Purified Pba1-Pba2 was dialyzed into specific buffers as required. A tagless variant of Pba1-Pba2 that had a PreScission protease (GE Healthcare) site inserted between the His_6 tag, and the N terminus of Pba2 was prepared by overnight dialysis in buffer A with the protease between the nickel-nitrilotriacetic acid and Q chromatography steps. Following cleavage, Pba2 has the additional N-terminal residues GlyPro. Selenomethionine-substituted Pba1-Pba2 was expressed as described (16) and purified in an identical manner to the native protein. The histidine tag was removed for crystallization trials and peptidase activity assays. The histidine tag was retained on samples used for the analytical ultracentrifugation and surface plasmon resonance (SPR) experiments shown here, although essentially identical SPR results were obtained with tagless proteins. 20S proteasome was prepared as described (17) using *S. cerevisiae* strain SDL135, which expresses proteasome subunit Pre1/β4 with protein A integrated at the C terminus.

Biosensor Binding Assays—Human IgG (Sigma-Aldrich) was immobilized on all four flow cells of a CM5 sensor chip in a Biacore 2000 instrument using standard amine coupling chemistry. Two g of pulverized yeast extract expressing the protein A-tagged proteasome was suspended in 10 ml of 20 mM Tris, pH 7.5, 0.1 mM EDTA, and 0.5 mM DTT for 10 min then centrifuged for 30 min at 14,000 × *g*. Proteasome from the clarified lysate was captured on the IgG surface at a variety of surface densities, each of which gave the same binding kinetics. Surfaces were washed by injection of running buffer (25 mM Tris, pH 7.5, 1 mM tris(2-carboxyethyl)phosphine) containing first 500 mM NaCl for 10 min followed by 1 M NaCl for an additional 10 min. Pba1-Pba2 proteins were assayed in a 3-fold dilution series in buffers containing 20 mM Tris, pH 7.5, 1 mM tris(2-carboxyethyl)phosphine, 0.01% P20, 0.1 mg/ml BSA, and either 12.5, 50, or 150 mM NaCl. All data were collected at 25 °C and processed using ScrubberPro6 (Biologic Software Pty, Ltd., Campbell, Australia). Response data were normalized using the R_{max} for each data set and globally fit to a 1:1 interaction model.

Genetic Analyses—Yeast strains isogenic with the A364a genetic background (supplemental Table S2) were grown to saturation in rich medium, and then aliquots of 10-fold serial dilutions were placed on different media and incubated under the conditions shown for 2 days (3 days for plates containing canavanine). Strains were tested for stability of mitochondrial function using the triphenyltetrazolium chloride (tetrazolium red) overlay method (18). Briefly, strains were grown on rich medium with glycerol as the sole carbon source to select for maintenance of mitochondrial function, and then independent clones were grown to saturation in rich medium containing 2% glucose. Dilutions were plated on rich glucose medium and plates with 50–300 individual colonies were stained with 0.1% triphenyltetrazolium chloride in an agar overlay. The percentage of colonies that failed to stain and therefore lacked mitochondrial function was determined.

Crystallography and Structure Analysis—Pba1-Pba2 and proteasome were dialyzed overnight against 10 mM Tris-HCl, pH 7.4, 1 mM EDTA, and 1 mM tris(2-carboxyethyl)phosphine, and concentrated by ultrafiltration to ~10 mg/ml and 6–9 mg/ml, respectively. MG132 (50 mM stock in dimethyl sulfoxide) was added in a 200× molar excess to the 20S proteasome and incubated at 4 °C for 30 min, and the solution was centri-

[5] The abbreviations used are: Hb*YX*, hydrophobic-tyrosine-any residue; PDB, Protein Data Bank; SPR, surface plasmon resonance.

fuged at 14,000 × *g* for 10 min. The supernatant was carefully isolated and added to a 2.5-fold molar excess of Pba1-Pba2. Following a 30-min incubation at 4 °C, samples were centrifuged as above prior to crystallization by the sitting drop method at 4 °C with a drop of 4 μl of precipitant (0.1 M sodium citrate (pH 5.5–5.7) and 18–20% PEG 3000) and 2 μl of Pba1-Pba2 proteasome solution. Crystals were briefly transferred to precipitant solution made up with 30% glycerol (cryoprotection buffer), suspended in a loop, and cooled by plunging into liquid nitrogen. The mercury derivative was prepared by soaking a crystal in cryoprotection buffer supplemented with 1 mM thimerosal for 6 h prior to cooling. Diffraction data were collected at beamline X29 of the National Synchrotron Light Source and processed using HKL2000 (19). Phases were determined by molecular replacement using PHASER (20) and half of the unliganded proteasome structure (Protein Data Bank code 1RYP) (21) as a search model. The first 30 residues of the α-subunits were omitted from the search model. Model building was facilitated by anomalous difference Fourier maps that localized selenomethionine and cysteine (mercury derivative) positions. Model building, structure refinement, and validation were accomplished using COOT (22), PHENIX (23), and MolProbity (24), respectively. Statistics are given in supplemental Table S1. The following residues lack interpretable density and have been omitted from the refined model: Pba1 (residues 1–27, 39–46, 79–119) and Pba2 (residues 125–181, 193–203, 232–240).

Molecular figures and overlaps were generated using University of California, San Francisco CHIMERA (25). Molecular interfaces were analyzed using PDBsum (26). Overlap of different proteasome structures was performed by superposition of the β-rings. The overlays of Pba1 and Pba2 tails shown in Fig. 4, *B* and *E*, were achieved by superposing equivalent structural elements that line the α5/α6 and α6/α7 pockets. Paired sequences used for superposition are (α5(17–30;155–172), α6(20–35;74–81)), and (α6(15–28;144–161), α7(21–36;77–84)) for the α5/α6 and α6/α7 pockets, respectively.

20S Proteasome Activity Assay—100-μl reactions were performed in 96-well plates using a Polarstar Optima (BMG Labtech) fluorometer. 100 ng (1.35 nM) of yeast 20S proteasome and either 20 ng (3.18 nM) of Pba1-Pba2 or 59.5 ng (3.18 nM) of PA26 were preincubated in 50 μl of assay buffer (20 mM Tris, pH 7.5, 25 mM NaCl, 1 mM DTT) at 30 °C for 12 min prior to adding the substrate Suc-LLVY-AMC (Enzo Life Sciences) to a final concentration of 100 μM. Following the addition of substrate, fluorescence was read every 5 min for 1 h. Experiments were conducted at 30 °C. Fluorescence/min was calculated using values within the linear range ($n = 6$ for each sample). Control reactions included 20S proteasome only, Pba1-Pba2 only, and PA26 only.

RESULTS

Pba1-Pba2 Binds the Mature 20S Proteasome—S. cerevisiae Pba1 and Pba2 proteins were coexpressed in bacteria, purified, and shown to form a monodisperse heterodimer by equilibrium analytical ultracentrifugation (supplemental Fig. S1). To assay Pba1-Pba2 interactions with the mature 20S proteasome, we used SPR (14). These data indicate a dissociation constant (K_D) of 2.78 ± 0.02 μM in a buffer containing 150 mM NaCl and an interaction model in which one Pba1-Pba2 heterodimer binds to each end of the proteasome, consistent with the crystal structure (see below). The interaction was salt-sensitive, with binding affinity increasing to $K_D = 68.1 \pm 0.4$ nM and $K_D = 12.17 \pm 0.04$ nM in buffers containing 50 mM or 12.5 mM NaCl, respectively (Fig. 1). In contrast to a recent study on the apparent archaeal homologs of Pba1-Pba2 (15), inhibition of the proteasome proteolytic sites with either MG132 or *clasto*-lactacystin β-lactone had no effect on the binding affinity or kinetics of Pba1-Pba2 (supplemental Fig. S2).

Pba1-Pba2 C Termini Function in Binding—Removing the three C-terminal HbY*X* residues of Pba1 (Pba1ΔCT) gave more than 150-fold reduction in binding affinity in 12.5 mM NaCl and undetectable binding in 150 mM NaCl (Fig. 1). Mutation of the Pba1 HbY*X* tyrosine or hydrophobic residue resulted in similar changes in affinity. Each of these changes to C-terminal residues of Pba1 reduced affinity by both decreasing the association rate and increasing the dissociation rate. In contrast to the dramatic effects seen with Pba1, truncation or mutation of the Pba2 HbY*X* caused only modest (3- to 5-fold) reductions in affinity. As expected, the Pba2 variants displayed slower association rates, although unlike Pba1, the Pba2 variants also displayed slower dissociation rates. Moreover, heterodimers bearing mutations in both Pba1 and Pba2 HbY*X* motifs displayed binding kinetics similar to variants containing mutations only in Pba1. Thus, although both Pba1 and Pba2 HbY*X* motifs contribute to binding, that of Pba1 makes a larger contribution and the mechanisms are different.

The C Termini of Pba1-Pba2 Contribute to Their Physiological Activity, Including a Role in Maintaining Mitochondrial Function—To determine the importance of the HbY*X* motifs of Pba1 and Pba2 to their biological function, we analyzed the phenotypes of mutants in *S. cerevisiae*. Consistent with previously published reports (7, 8), deleting the entire open reading frames of both *PBA1* and *PBA2* did not cause a significant growth defect, but triple mutants lacking Pba1-Pba2 and Rpn4 (the transcription factor that regulates expression of many proteasomal proteins; *pba1*-Δ, *pba2*-Δ, *rpn4*-Δ) failed to grow at elevated temperatures or in the presence of low levels of canavanine (which leads to synthesis of aberrant proteins and therefore to an increase in the need for proteasomal function; Fig. 2*A*, *top row*). Pba1 and Pba2 each perform unique functions because deleting either gene in a strain lacking Rpn4 caused defective growth. Strains with deletions of the final three Pba1-Pba2 C-terminal residues or with the penultimate tyrosines mutated to alanine were essentially as defective as full gene deletions (Fig. 2*A*, *middle* and *bottom rows*). Although deletion of either C terminus was sufficient to cause an *rpn4*-Δ strain to fail to grow at 38 °C, deletion of both C termini was required to produce the full growth defect at 37 °C (supplemental Fig. S3). These results support the recently reported finding that the C-terminal HbY*X* motifs of Pba1 and Pba2 are at least partially redundant with one another *in vivo* (15) but also shows that each has a unique function. Together, these results show that an important biological function of Pba1-Pba2 requires the action of the HbY*X* motifs of both proteins, matching the roles of each motif in binding to proteasomes *in vitro*.

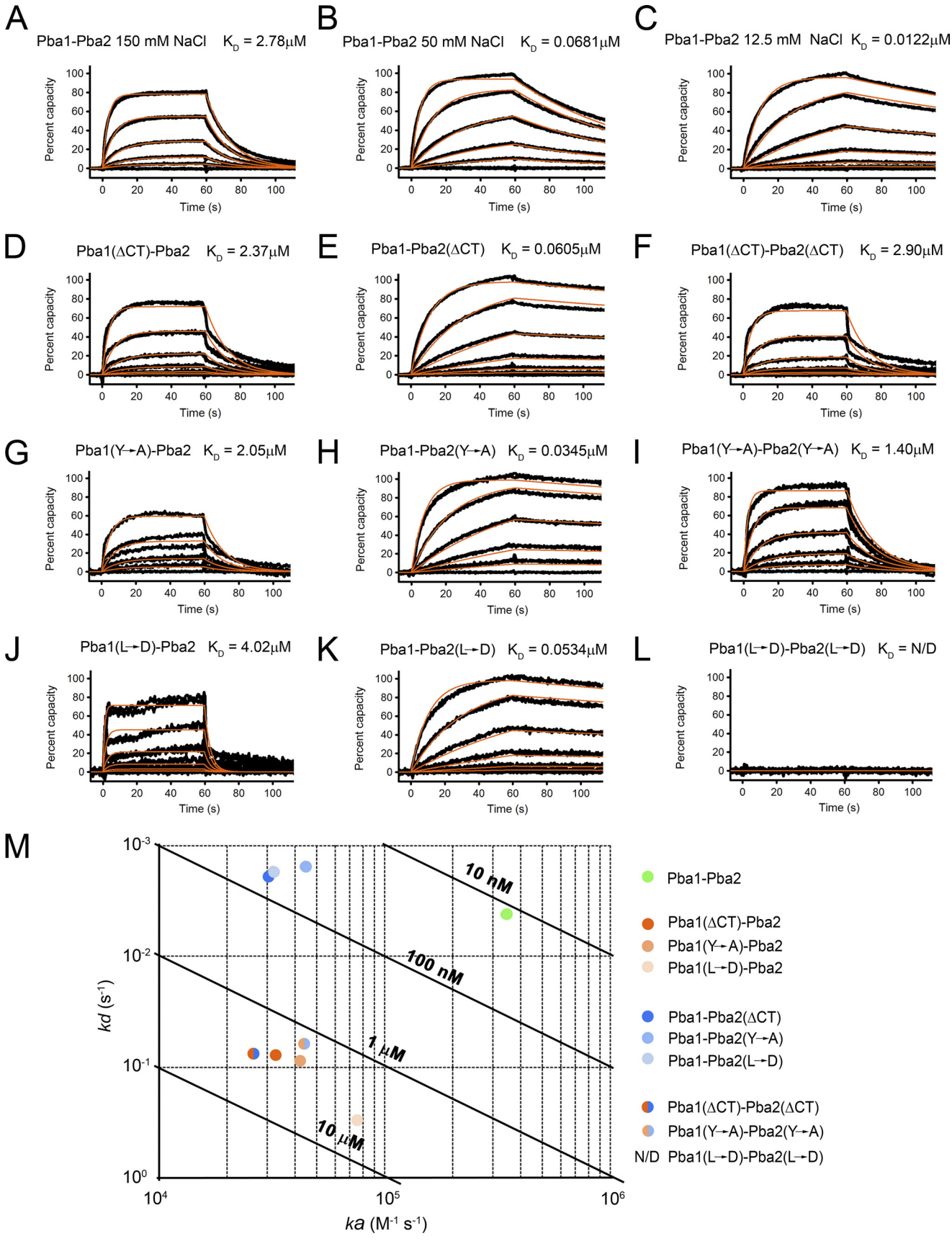

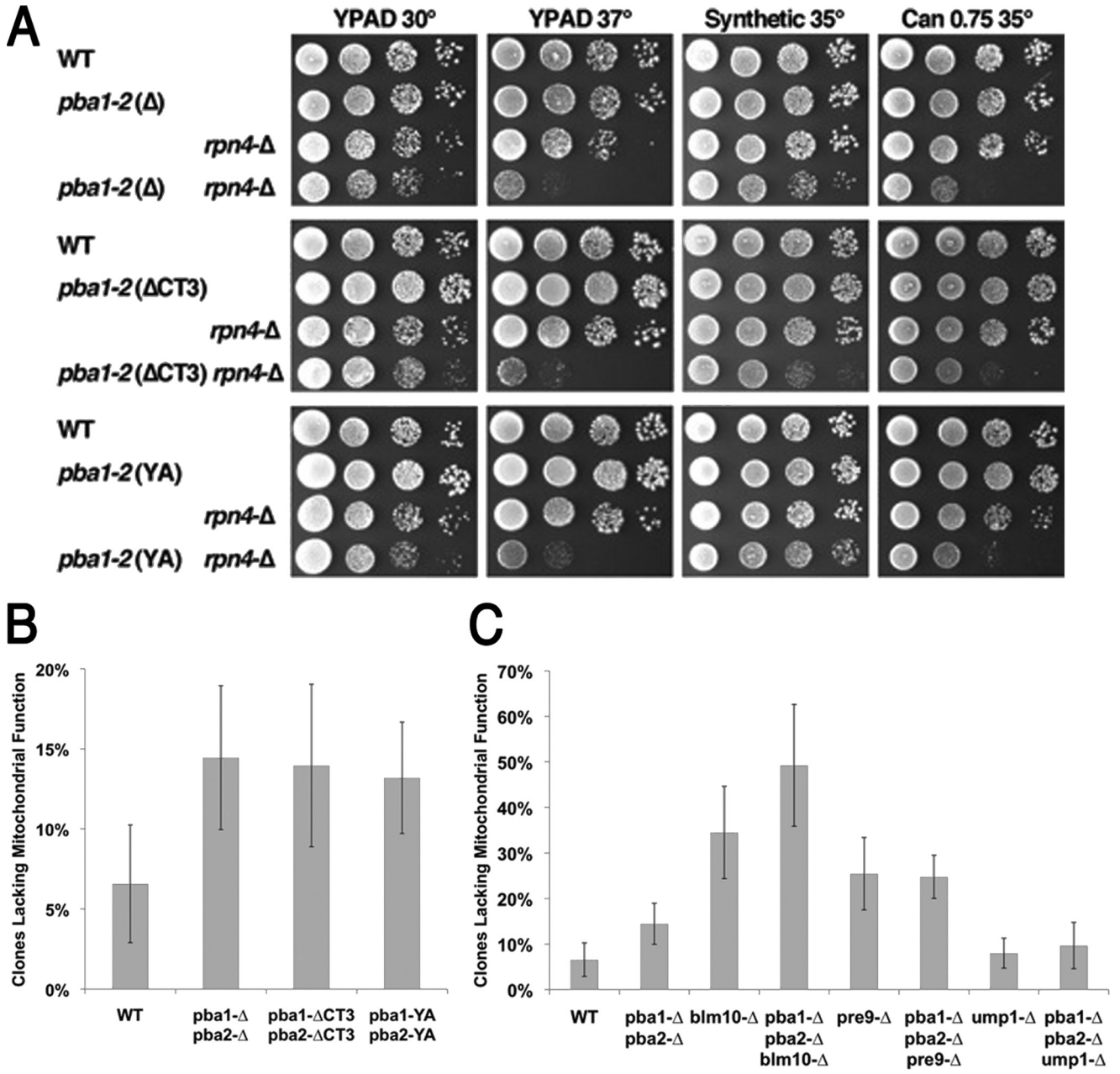

FIGURE 2. **Physiological functions of Pba1-Pba2 require intact C termini and affect the stability of mitochondrial function.** *A*, 10-fold serial dilutions of isogenic yeast strains (supplemental Table S2) were tested as described under "Experimental Procedures." *pba1*-Δ, *pba2*-Δ, and *rpn4*-Δ indicate complete deletion of the ORFs. *pba1–2*Δ and *pba1–2*ΔCT3 indicate deletion of the complete ORFs or the final three residues of both ORFs. *pba1–2 YA* indicates mutation of the penultimate tyrosine of both ORFs to alanine. The ΔCT and YA mutations were constructed by integrating *LEU2* or *URA3* 30 bp downstream of the open reading frame using a primer that introduced a premature stop codon or the Tyr-to-Ala mutation, so that all expression is from the native promoter in a genomic context. *YPAD* indicates rich medium, *synthetic* indicates synthetic medium lacking arginine, and *Can 0.75* is synthetic medium lacking arginine and containing 0.75 μg/ml of the arginine analog canavanine. *B* and *C*, isogenic strains with the relevant genotypes shown were grown on rich medium then tested for mitochondrial function by staining with the dye triphenyltetrazolium chloride as described (18). The average and standard deviation of the percentage of clones displaying loss of mitochondrial function in multiple (at least five) independent repeats of this assay is graphed.

We expanded the genetic analysis by assaying the importance of Pba1-Pba2 for maintaining mitochondrial function. Previous studies have shown a role for the 19S regulatory complex (27) and the proteasome assembly chaperone Ump1 (28) in mitochondrial function, and we have previously shown that the proteasome binding partner Blm10 functions in a mitochon-

FIGURE 1. **Pba1-Pba2 binds mature 20S proteasomes using the HbY*X* motifs.** *A*, sensorgrams for binding of Pba1-Pba2 to immobilized proteasomes showing normalized response (*black*) and binding models (*red*) in 150 mM NaCl. *B*, 50 mM NaCl. *C*, 12.5 mM NaCl. *D–L*, performed as for *C* in 12.5 mM NaCl. *D*, with Pba1 HbY*X* deleted. *E*, with Pba2 HbY*X* deleted. *F*, Pba1 and Pba2 HbY*X* deleted. *G*, Pba1 HbY*X* Tyr→Ala substitution. *H*, Pba2 HbY*X* Tyr→Ala substitution. *I*, Pba1 and Pba2 HbY*X* Tyr→Ala substitutions. *J*, Pba1 HbY*X* Leu(Hb)→Asp substitution. *K*, Pba2 HbY*X* Leu(Hb)→Asp substitution. *L*, Pba1 and Pba2 HbY*X* Leu(Hb)→Asp substitutions. *M*, kinetic plot of k_a *versus* k_d for all Pba1-Pba2 variants in 12.5 mM NaCl. *Diagonals* represent constant K_D values. In all cases, the standard deviation is less than the size of the spots. *N/D*, not detected.

drial checkpoint pathway (13). Yeast cells can grow in the absence of mitochondrial oxidative phosphorylation if they are provided with a fermentable carbon source such as glucose but are unable to metabolize glycerol or other non-fermentable carbon sources, and the resulting colonies fail to stain with the dye triphenyltetrazolium chloride (18). Growth of a normal strain in glucose-containing medium results in the accumulation of a surprisingly high number of cells that have lost this mitochondrial function (6.4 ± 3.4% for the 39 independent clones shown in Fig. 2*B*). Complete deletion of *PBA1-PBA2*, deletion of just the HbY*X* motifs or mutation of the penultimate tyrosines to alanines all produced essentially the same destabilization of mitochondrial function, resulting in a 2.2-fold increase in the yield of cells lacking mitochondrial function (Fig. 2*B*). Other proteasome-related factors also contributed to maintenance of mitochondrial function, with more subtle effects (*rpn4*-Δ caused a 1.2-fold increase; Fig. 2*C*) or more dramatic ones (loss of the proteasome α3 subunit in a *pre9*-Δ strain caused a 4.0-fold increase, and loss of Blm10 caused a 5.4-fold increase; Fig. 2*C*) (13). Combining mutations in these factors revealed complex genetic interactions, with the phenotype of Pba1-Pba2 deletion being enhanced by simultaneous loss of Blm10 or Rpn4, but not by loss of Pre9 or Ump1. Pba1 and Pba2 also contributed unique activities to this function, as single mutants alone or combined with *rpn4*-Δ caused rates of mitochondrial function loss similar to the double *pba1*-Δ*pba2*-Δ mutant (supplemental Fig. S4). The relationship between proteasome activity and the stability of mitochondrial function remains unknown, but these results show that different features of proteasomes contribute in distinct, genetically complex ways, and confirm the importance of the C termini of Pba1 and Pba2 in all of their known physiological roles.

Pba1-Pba2 Proteasome Crystal Structure—We have determined a crystal structure of the Pba1-Pba2 proteasome complex at 2.5 Å resolution with an R_{free} value of 23.2% (Fig. 3 and supplemental Table S1). A single Pba1-Pba2 heterodimer binds each proteasome α-ring, and a 2-fold axis bisects the complex to yield a half-proteasome and one Pba1-Pba2 in the asymmetric unit.

Pba1-Pba2 Structure—Pba1 and Pba2 share similar overall topologies, with a β-sheet of four parallel strands that is extended by antiparallel strands and flanked on both faces by helices. They superpose with a root mean square deviation of 2.5 Å over 98 pairs of equivalent Cα atoms (Fig. 3*B*), although only eight of the structurally equivalent residues have the same amino acid identity, and there is considerable divergence in the lengths of loops between secondary structural elements.

Within the heterodimer, Pba1 and Pba2 are related to each other by an ~80° rotation, with both C termini extending away from the core, albeit to different extents and in different relative directions. The interface between Pba1 and Pba2 covers ~2,600 Å^2 and includes multiple van der Waals contacts and 12 hydrogen bonds (Fig. 3*C*). Conserved residues of Pba1 and Pba2 are mostly limited to the heterodimer core and the proteasome interface (Fig. 3*D*).

Proteasome Structure and MG132 Binding—Apart from the N-terminal gating residues of α-subunits (below), little conformational change is detected in the proteasome upon binding Pba1-Pba2. Following superposition on the proteasome β-subunits, the root mean square deviation between Pba1-Pba2-bound and unbound proteasome α-rings (PDB code 1RYP) (21) is ~1.0 Å over all corresponding pairs of Cα atoms, excluding the gate region (residues 1–30 of all α-subunits).

Crystals were grown in the presence of the inhibitor MG132, which primarily inhibits the β5 active site (29). We observe interpretable MG132 density only at the β5 site, where MG132 binding is consistent with proteasome complexes with related inhibitors (21, 30) and induces only modest conformational changes compared with the unliganded proteasome (21).

Despite multiple attempts over a wide range of conditions, only very poor crystals whose diffraction could not be indexed were obtained in the absence of an inhibitor or in the presence of *clasto*-lactacystin β-lactone. We therefore searched for map features indicating that a second MG132 molecule might mediate a lattice contact. We did not find suggestive density, although a lattice-stabilizing role for a partially ordered MG132 molecule cannot be completely ruled out.

The Interface between Pba1-Pba2 and the Proteasome—The extensive ~7,100 Å^2 interface of Pba1-Pba2 with the proteasome includes roughly equal contributions from Pba1 and Pba2 and contains 27 hydrogen bonds. Pba1 and Pba2 each make substantial contacts with subunits α5 and α6, whereas Pba1 also makes a small contact with α4, and Pba2 makes a substantial contact with α7 (Fig. 3*C*). The interface is highly convoluted. The N-terminal residues of α5 and α6 project away from the proteasome into a pocket formed at the Pba1-Pba2 interface that displays a relatively high fraction of conserved Pba2 residues, and the C-terminal residues of Pba1 and Pba2 insert into pockets formed between α-subunits (Fig. 4).

Interactions of the Pba1 and Pba2 HbY*X* motifs are of special interest (Fig. 5). The Pba1 HbY*X* binds the α5/α6 pocket where it overlaps closely with the C-terminal residues of bound Blm10 (Fig. 5, *A* and *C*) (13) and PA26 (31), with the terminal carboxylate forming a salt bridge with the pocket lysine (α6 Lys-62) and main chain groups forming antiparallel β-sheet-like hydrogen bonds with α6 Gly-76 and Ala-78. The Pba1 HbY*X* tyrosine lies in an equivalent position to that of Blm10, although its OH group forms a hydrogen bond with the NH group of α5 Leu-21 rather than with the O of α5 Gly-19 as seen with Blm10. This allows the tyrosine OH to also hydrogen bond with the α5 Glu-25 carboxylate, which is constrained by other interactions with Pba1. Curiously, Pba1 Glu-222 is superimposable with the "activation loop" glutamate of PA26 (32) and hydrogen bonds with residues on the proteasome α5 Pro-17 reverse turn, although this residue is conserved only in fungi, and we found only a modest reduction in binding affinity and no apparent phenotype when it was mutated to alanine.

The Pba2 HbY*X* binds the adjacent α6/α7 pocket and also forms a salt bridge with the pocket lysine (α7 Lys-65) but adopts a distinct conformation and forms different interactions from those of Pba1, Blm10, and PA26 (Fig. 5, *B* and *D*). The distinct HbY*X* conformations can be explained by differences in the Pba1 and Pba2 amino acid sequences. Pba1 and Pba2 approach their pockets from different orientations but enter the pocket as structurally equivalent helices (Fig. 5*E*), after which Pba1 has a

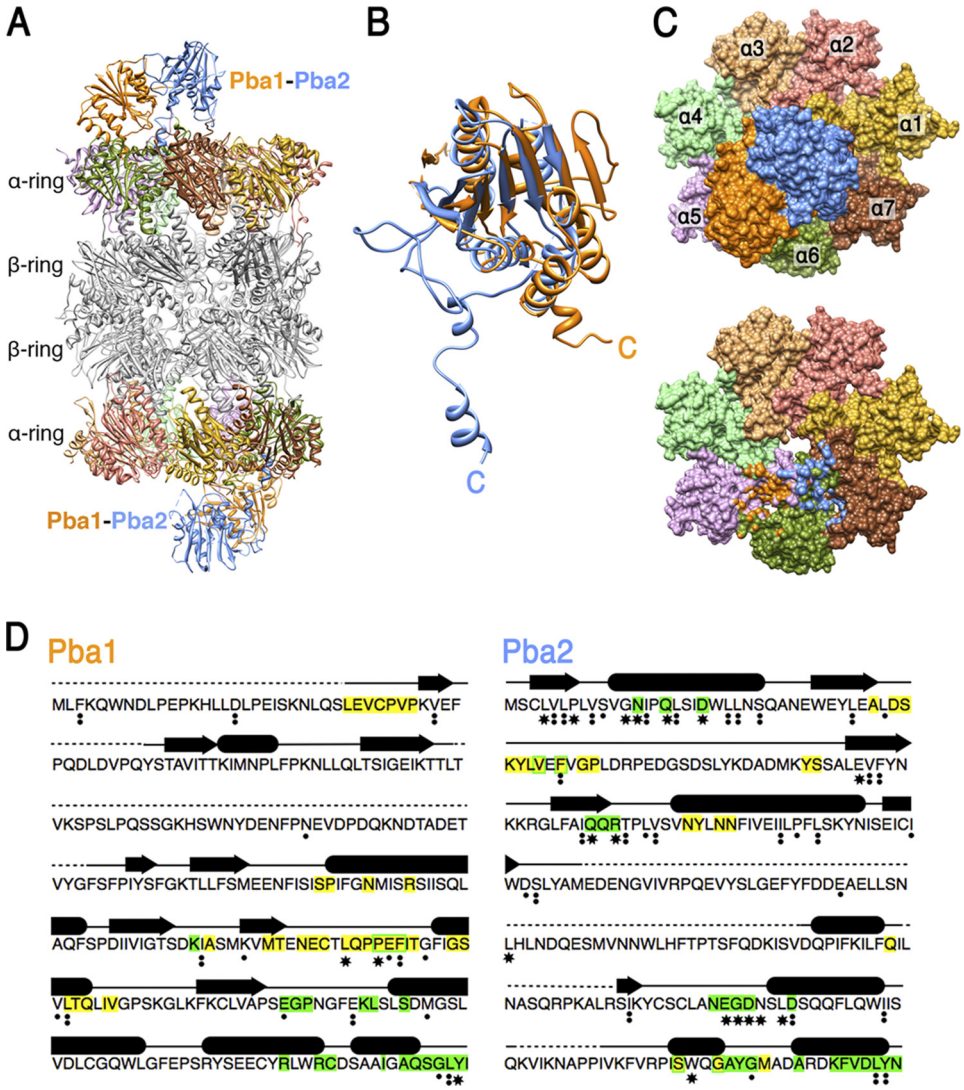

FIGURE 3. **Structure of the Pba1-Pba2 proteasome complex.** *A*, ribbon diagram viewed from the *side*. Pba1, Pba2, and proteasome α- and β-subunit rings are labeled. Different orientations are apparent for the Pba1-Pba2 heterodimers at either end of the complex because the proteasome 2-fold molecular axis is offset ~45° from the view direction. *B*, superposition of Pba1 and Pba2 following an overlap of their structures that emphasizes similarity within secondary structural elements. C termini are labeled. *C*, *top view* of the complex in space-filling representation (*upper panel*) and with Pba1-Pba2 removed (*lower panel*). In the *lower panel*, proteasome surface in contact with Pba1 and Pba2 is colored *orange* and *blue*, respectively. *D*, *S. cerevisiae* Pba1 and Pba2 sequences with observed secondary structure above and disordered regions *dotted*. Residue conservation in eukaryotic species (six chordata and seven fungi) is denoted in Clustal format: conserved (*period* in *boldface type*), strongly conserved (*colon* in *boldface type*), and invariant (*asterisk* in *boldface type*) (41). Residues that mediate contacts at the interfaces between Pba1 and Pba2 and between Pba1-Pba2 and the proteasome are colored *yellow* and *green*, respectively.

single residue (Gly-273) insertion that makes Pba1 Leu-274 (HbY*X*) equivalent to Pba2 Tyr-266 (Hb*Y*X). Another important difference is seen between the structurally equivalent Pba1 Gly-269 and Pba2 Phe-262 residues because the large Pba2 Phe-262 side chain prevents the HbY*X* tyrosine from adopting the canonical conformation of Pba1. Thus, residues N-terminal to the HbY*X* motifs explain why the Pba1-Pba2 C-terminal Cα atoms are shifted by 3.8 Å in this overlap, why the Pba2 HbY*X* does not form hydrogen bonds equivalent to those of Pba1, and why the Pba2 HbY*X* tyrosine OH group is 4.2 Å from the closest potential hydrogen bond partner.

The Pba1-Pba2-bound Proteasome Gate Is Partially Displaced and Is Functionally Closed—Pba1-Pba2 forms a cup-like structure over the center of the proteasome α-ring, leaving the pore visible only when viewed from an oblique angle (Fig. 6*A*). The N-terminal residues of α5, α6, and α7 make extensive contacts with Pba1-Pba2 and are therefore more ordered than in the unliganded proteasome (Fig. 6, *A* and *C*). In contrast, the α1, α2, α3, and α4 N-terminal residues display more disorder in the complex with Pba1-Pba2, including for some residues that seal the gate in the absence of a binding partner (Fig. 6, *B* and *C*). Although this means that a channel is visible when disordered residues are not displayed (Fig. 6*C*), the channel is far from the fully open conformation seen with PA26 (31, 32) and exhibits substantially less disorder than seen in the Blm10-bound state (13). Indeed, the channel appears too narrow and occluded by disordered residues to allow passage of even small peptides (Fig. 6*B*).

To test the structural implication that the proteasome gate is functionally closed in the Pba1-Pba2 complex, we performed

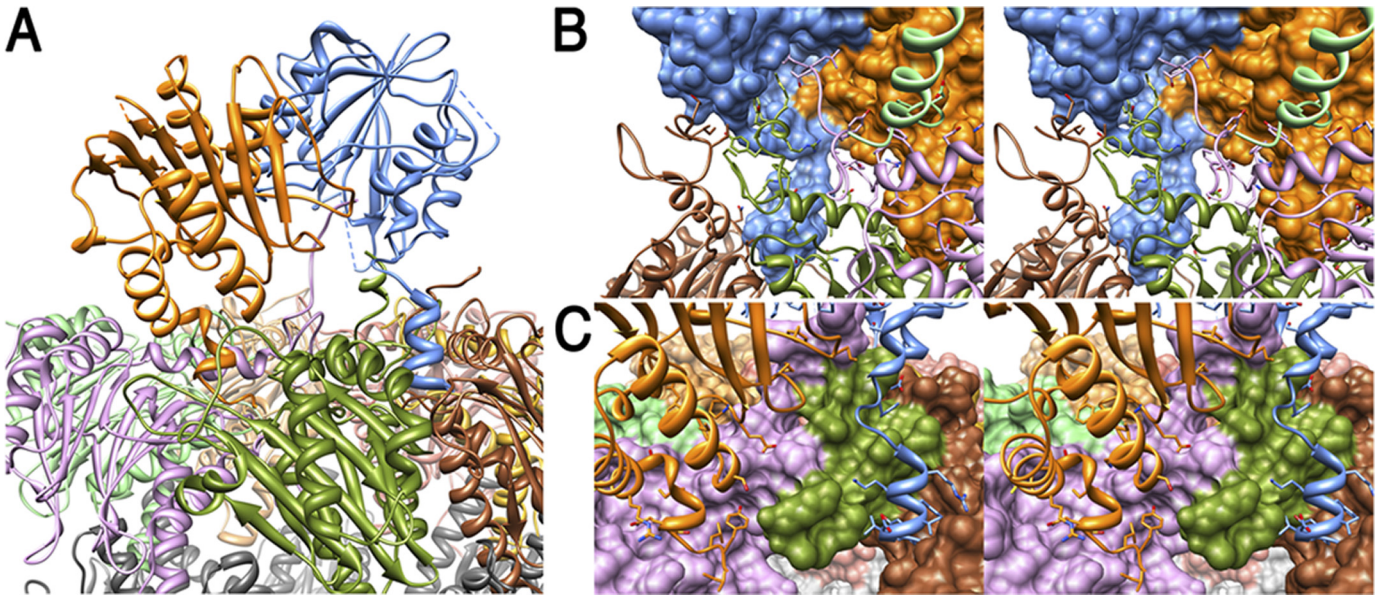

FIGURE 4. **The interface between Pba1-Pba2 and the proteasome.** *A*, Pba1 and Pba2 C termini insert into proteasome pockets and α5 and α6 N termini insert into a pocket on Pba1-Pba2. *B*, *cross-eye stereoview* of α4(1–30), α5, α6, and α7 shown as ribbons and the Pba1-Pba2 molecular surface. The view direction is approximately opposite from that of *A*. *C*, proteasome molecular surface (only the first 30 residues of α6 are shown for clarity) and Pba1-Pba2 represented as ribbons. The view direction is tilted with respect to *A*.

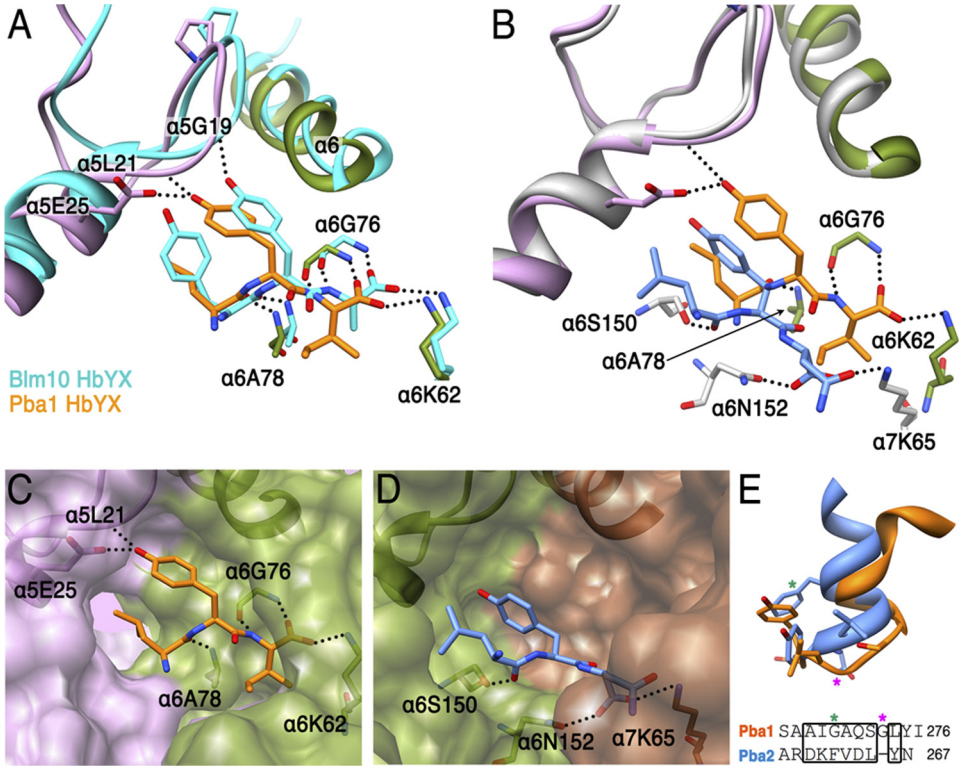

FIGURE 5. **Conformations and interactions of the HbY*X* motifs.** *A*, Pba1 and Blm10 C-terminal HbY*X* tripeptides and surrounding proteasome residues are shown following overlap on β-subunits. Pba1 and associated α5 and α6 residues are colored as for other figures. Blm10 and associated proteasome residues are colored *cyan*. *B*, superposition of Pba1 and Pba2 and their surrounding proteasome residues following superposition on equivalent structural elements lining the pockets. Standard colors are used for Pba1. Pba2 is colored *blue*, and its associated proteasome residues are colored *white*. *C*, surface representation of the proteasome with Pba1 HbY*X* residues shown as sticks, and H-bonding interactions are shown as *dotted lines*. *D*, equivalent to *C* but for the Pba2 HbY*X* residues. *E*, Pba1 and Pba2 C-terminal residues superposed as for *B*. Structurally equivalent residues (defined as Cα within 3 Å) are *boxed* in the sequence alignment. Pba1 Gly-269 and Pba2 Phe-262 are indicated with *pink* and *green asterisks*, respectively.

biochemical hydrolysis assays. Consistent with a recent report (15), we failed to detect enhanced proteasomal hydrolysis of the fluorogenic peptide Suc-LLVY-AMC in the presence of Pba1-Pba2 (Fig. 7*A*). We also tested the hypothesis that Pba1-Pba2 is a 20S proteasome substrate (6) but found no evidence for this upon prolonged incubation (Fig. 7, *B–D*). These findings are consistent with the model that the proteasome pore is occluded when bound with Pba1-Pba2.

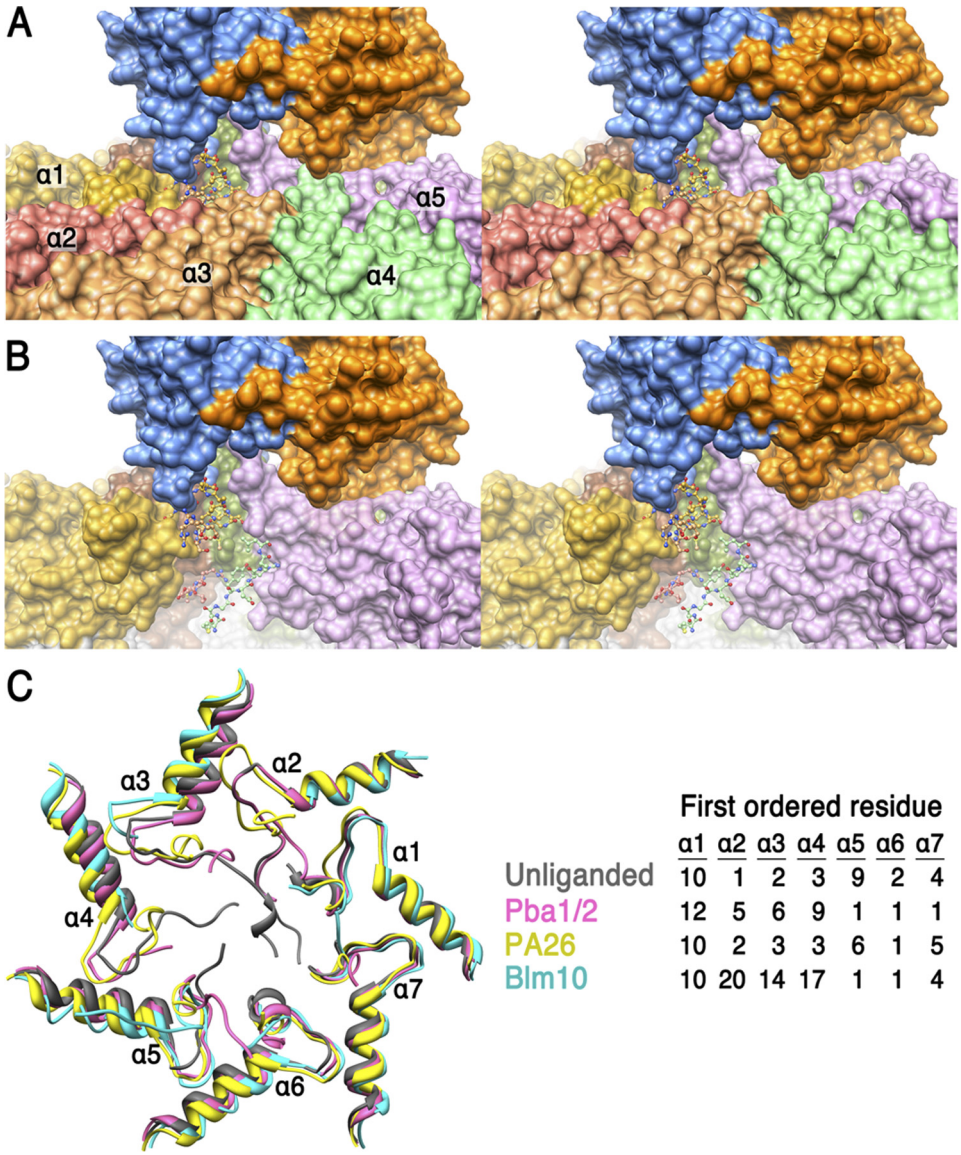

FIGURE 6. **Proteasome gate conformation.** *A*, space-filling stereoview representation of the opening to the proteasome pore. Disordered gate residues (α1(1–11), α2(1–4), α3(1–5), α4(1–8)) are built in stereochemically reasonable conformations and shown in ball-and-stick representation. *B*, same view as *A* but with the ordered residues of α2, α3, and α4 removed to visualize the pore interior. *C*, yeast proteasome pore conformations. Unliganded (*gray*, PDB code 1RYP), in complex with PA26 (*yellow*, PDB code 1Z7Q), Blm10 (*cyan*, PDB code 1VSY), and Pba1-Pba2 complex (*pink*). Disordered residues are not shown. The first ordered residues are tabulated.

DISCUSSION

Mature 20S proteasomes have a variety of binding partners that display radically different architectures but utilize similar modes of binding through their C-terminal residues (10). Multiple C termini of the heptameric 11S activators form salt bridge and hydrogen bonding interactions with proteasome α-subunit pockets (31) and superimposable interactions are observed with the one C terminus of the monomeric Blm10 protein (13). 11S and Blm10 induce full or partial opening of the proteasome gate, respectively, by repositioning the proteasome Pro-17 reverse turn. An important element of the Blm10 interaction involves the penultimate tyrosine/phenylalanine residue, and equivalent interactions of penultimate tyrosine and surrounding residues also seem to be critical components of binding and gate opening by multiple subunits of the hexameric ATPase PAN/19S activators (14, 33).

Our structure determination shows that Pba1-Pba2 both preserves the characteristic mode of C-terminal binding and adds to the remarkable diversity of structurally defined proteasome-binding partners. Pba1-Pba2, which we show is a stable heterodimer, is architecturally quite different from 11 S, Blm10, and PAN/19S activators, with structural equivalence found only where the C-terminal residues of Pba1 bind to the α5/α6 pocket (Fig. 5). The Pba2 HbY*X* interaction lacks even this structural equivalence, using a similar motif in a divergent manner to bind the α6/α7 pocket. The less extensive interactions observed with Pba2 are consistent with the lack of conservation of these residues beyond fungal species (15) and their smaller contribution to binding (Fig. 1). However, both C-terminal tails do make significant contributions to the binding of Pba1-Pba2 to the proteasome *in vitro*, and both are important

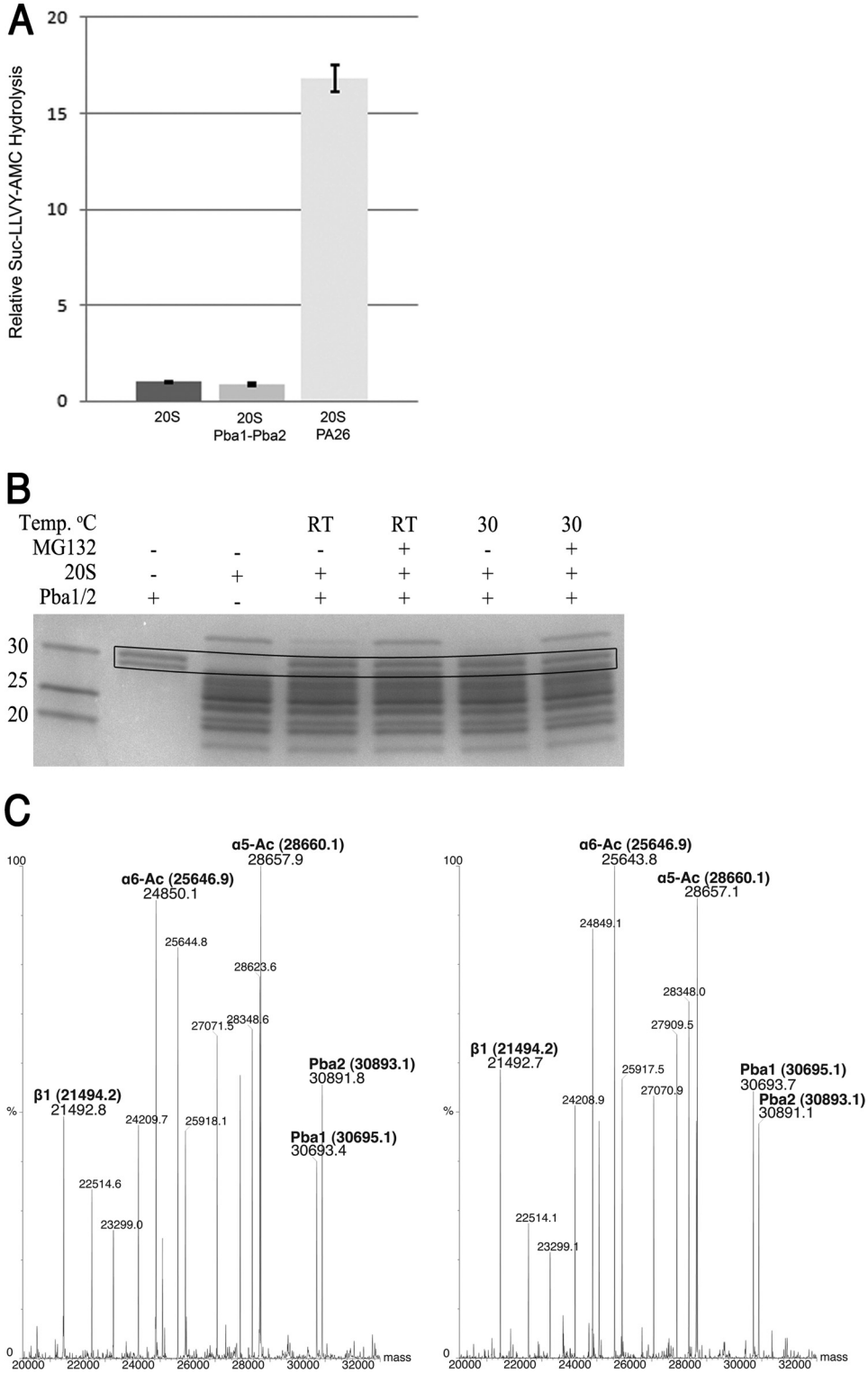

FIGURE 7. **Pba1-Pba2 does not activate the proteasome and is not a proteasome substrate.** *A*, Pba1-Pba2 does not stimulate hydrolysis of the model peptide substrate Suc-LLVY-AMC in conditions containing 25 mM NaCl, under which robust Pba1-Pba2 proteasome binding was observed in SPR assays. Samples containing 20S proteasome only, proteasome and Pba1-Pba2, or proteasome and PA26 were averaged ($n = 6$) and normalized to proteasome only reactions. *B*, Pba1-Pba2 is not a proteasome substrate *in vitro*. SDS-PAGE of Pba1-Pba2-proteasome incubated with and without MG132 for 24 h at 30 °C or room temperature (*RT*). Pba1-Pba2 and free 20S proteasome are shown for comparison. The bands corresponding to Pba1-Pba2 are *boxed* and do not change in intensity regardless of the inhibition state of 20S proteasome. The most slowly migrating band corresponds to α7, which is clipped upon incubation in the absence of MG132. *C*, ESI-MS spectra from the analysis of the 30 °C samples incubated in the absence (*left*) or presence (*right*) of MG132. Observed molecular weights are in normal font, and calculated values are in *boldface type* and *parentheses*. Pba1-Pba2 apparent abundance relative to proteasome components is similar in both samples. Apparent molecular weights indicate that α5 and α6 are acetylated, consistent with electron density at their N termini.

for the physiological roles of Pba1-Pba2 *in vivo*, including the maintenance of mitochondrial function. Although the Pba1 HbY*X* interaction is superimposable with activating interactions of Blm10 (13) and models of PAN/19S (14), our structural and biochemical data show that the proteasome entrance gate is closed in the presence of Pba1-Pba2 (Figs. 6 and 7A). Thus, despite conservation of the primary "activating" interaction, Pba1-Pba2 is not itself a proteasome activator and is not degraded by the purified 20S proteasome, thereby arguing against the previously attractive proposal that Pba1-Pba2 targets its own destruction upon completion of assembly (6). The persistent use of HbY*X* motifs for proteasome binding in otherwise highly divergent contexts raises the question of how many other functionally important proteasome binding partners exist, with one attractive candidate being PI31 (34, 35).

It is notable that the Blm10 C terminus also binds the α5/α6 pocket that is occupied by Pba1 (13) and that the C-terminal residues of the homoheptameric PA26 11S activator appear to bind four of the *S. cerevisiae* proteasome pockets, including α5/α6, but lack defined density in other pockets, including the α6/α7 pocket that is occupied by Pba2 (31). Cross-linking (36) indicates that the 19S Rpt5 subunit, which displays a C-terminal HbY*X*, can bind α5/α6, and electron microscopy (37) indicates that the Rpt5 C terminus binds α5/α6 but that α6/α7 is unoccupied in the 19S-bound proteasome. These observations emphasize the functional importance of the asymmetric structure of eukaryotic proteasomes, despite their pseudo-symmetric appearance.

It is established that Pba1-Pba2 functions in proteasome assembly (6–8). Using the Dali server (38), we find that Pba1 and Pba2 are structurally similar to PDB code 3GAA, which has been suggested to be an ortholog of the archaeal proteasome assembly factors PbaA and PbaB (15). Given that PbaA and PbaB only bind mature 20S proteasomes in the presence of an inhibitor (15), it was striking that we were only able to grow crystals in the presence of MG132. This is reminiscent of models in which binding at the proteolytic sites modulates the conformation at the apical surface of the α-subunits to stabilize association with the 19S activator (39) and to promote gate opening (40). The allostery model does not apply to Pba1-Pba2, however, because our SPR data show that binding kinetics are unchanged when proteasomes are inhibited with either MG132 or with *clasto*-lactacytsin β-lactone. Moreover, the close structural conservation within the body of the proteasome when unliganded and when bound to Pba1-Pba2 does not suggest a mechanism for communication between proteasome proteolytic sites and the apical surface. A more mundane possibility stems from our observation that MG132 inhibits post-purification processing/clipping of α7 (Fig. 7*B*), which may alter lattice contacts that are important for crystallization. The possibility of allosteric communication between proteolytic sites and the proteasome α-subunits and the extent to which the archaeal PbaA and PbaB proteins mimic the role of eukaryotic Pba1 and Pba2 remain important but unresolved questions.

Eukaryotic proteasome assembly initiates with α-ring formation, which is promoted by Pba1-Pba2 and the unrelated Pba3-Pba4 heterodimer (2). Pba3-Pba4 modulates incorporation of α3 and α4 and binds primarily to α5 on the surface that becomes occluded by β4, β5, and β6 in assembled proteasomes. This explains why Pba3-Pba4 is displaced as β-subunits are added during assembly (4, 5). In contrast, Pba1-Pba2 remains associated throughout all stages of 20S proteasome assembly (6–8), a finding that is consistent with several non-exclusive assembly mechanisms that are suggested by the complex structure: First, Pba1-Pba2 may dictate the appropriate arrangement of nucleating subunits through its direct contacts with α4, α5, α6, and α7. Second, the apical location of Pba1-Pba2 may sterically prevent the accumulation of α-ring dimers that have been observed upon disruption of Pba1-Pba2/PAC1-PAC2 in mammalian cells (6). Third, the structure may represent the final assembly intermediate in which sequestration of α5, α6, and α7 N termini in a conserved pocket of Pba1-Pba2 promotes formation of the intricate closed gate conformation by allowing the more buried α2 and α3 N-terminal residues to assume their correct relative positions. Fourth, Pba1-Pba2 may prevent premature association of nascent α-rings with activators, such as 19S. Thus, our data explain the association of Pba1-Pba2 throughout all stages of 20S proteasome assembly, including those with the fully assembled state represented by our structure.

Acknowledgments—We thank William Alexander, Zaily Connell, and Ira Baci for technical assistance. We thank Mark Hochstrasser and Andrew Kusmierczyk for insightful discussions and for providing Pba1 and Pba2 template DNA that was used to generate the expression vector used in these studies. Data collection at the National Synchrotron Light Source was funded by the National Center for Research Resources. Operations of the National Synchrotron Light Source are supported by the United States Department of Energy, Office of Basic Energy Sciences, and by the National Institutes of Health.

REFERENCES

1. Pickart, C. M., and Cohen, R. E. (2004) Proteasomes and their kin: proteases in the machine age. *Nat. Rev. Mol. Cell Biol.* **5,** 177–187
2. Murata, S., Yashiroda, H., and Tanaka, K. (2009) Molecular mechanisms of proteasome assembly. *Nat. Rev. Mol. Cell Biol.* **10,** 104–115
3. Ramos, P. C., Höckendorff, J., Johnson, E. S., Varshavsky, A., and Dohmen, R. J. (1998) Ump1p is required for proper maturation of the 20S proteasome and becomes its substrate upon completion of the assembly. *Cell* **92,** 489–499
4. Yashiroda, H., Mizushima, T., Okamoto, K., Kameyama, T., Hayashi, H., Kishimoto, T., Niwa, S., Kasahara, M., Kurimoto, E., Sakata, E., Takagi, K., Suzuki, A., Hirano, Y., Murata, S., Kato, K., Yamane, T., and Tanaka, K. (2008) Crystal structure of a chaperone complex that contributes to the assembly of yeast 20S proteasomes. *Nat. Struct. Mol. Biol.* **15,** 228–236
5. Kusmierczyk, A. R., Kunjappu, M. J., Funakoshi, M., and Hochstrasser, M. (2008) A multimeric assembly factor controls the formation of alternative 20S proteasomes. *Nat Struct Mol. Biol* **15,** 237–244
6. Hirano, Y., Hendil, K. B., Yashiroda, H., Iemura, S., Nagane, R., Hioki, Y., Natsume, T., Tanaka, K., and Murata, S. (2005) A heterodimeric complex that promotes the assembly of mammalian 20S proteasomes. *Nature* **437,** 1381–1385
7. Le Tallec, B., Barrault, M. B., Courbeyrette, R., Guérois, R., Marsolier-Kergoat, M. C., and Peyroche, A. (2007) 20S proteasome assembly is orchestrated by two distinct pairs of chaperones in yeast and in mammals. *Mol. Cell* **27,** 660–674
8. Li, X., Kusmierczyk, A. R., Wong, P., Emili, A., and Hochstrasser, M. (2007) β-Subunit appendages promote 20S proteasome assembly by overcoming an Ump1-dependent checkpoint. *EMBO J.* **26,** 2339–2349
9. Sasaki, K., Hamazaki, J., Koike, M., Hirano, Y., Komatsu, M., Uchiyama, Y.,

Tanaka, K., and Murata, S. (2010) PAC1 gene knockout reveals an essential role of chaperone-mediated 20S proteasome biogenesis and latent 20S proteasomes in cellular homeostasis. *Mol. Cell. Biol.* **30,** 3864–3874
10. Stadtmueller, B. M., and Hill, C. P. (2011) Proteasome activators. *Mol. Cell* **41,** 8–19
11. Smith, D. M., Chang, S. C., Park, S., Finley, D., Cheng, Y., and Goldberg, A. L. (2007) Docking of the proteasomal ATPases' carboxyl termini in the 20S proteasome's α ring opens the gate for substrate entry. *Mol. Cell* **27,** 731–744
12. Gillette, T. G., Kumar, B., Thompson, D., Slaughter, C. A., and DeMartino, G. N. (2008) Differential roles of the COOH termini of AAA subunits of PA700 (19 S regulator) in asymmetric assembly and activation of the 26 S proteasome. *J. Biol. Chem.* **283,** 31813–31822
13. Sadre-Bazzaz, K., Whitby, F. G., Robinson, H., Formosa, T., and Hill, C. P. (2010) Structure of a Blm10 complex reveals common mechanisms for proteasome binding and gate opening. *Mol. Cell* **37,** 728–735
14. Stadtmueller, B. M., Ferrell, K., Whitby, F. G., Heroux, A., Robinson, H., Myszka, D. G., and Hill, C. P. (2010) Structural models for interactions between the 20S proteasome and its PAN/19S activators. *J. Biol. Chem.* **285,** 13–17
15. Kusmierczyk, A. R., Kunjappu, M. J., Kim, R. Y., and Hochstrasser, M. (2011) A conserved 20S proteasome assembly factor requires a C-terminal HbY*X* motif for proteasomal precursor binding. *Nat. Struct. Mol. Biol.* **18,** 622–629
16. Studier, F. W. (2005) Protein production by auto-induction in high density shaking cultures. *Protein Expr. Purif.* **41,** 207–234
17. Leggett, D. S., Hanna, J., Borodovsky, A., Crosas, B., Schmidt, M., Baker, R. T., Walz, T., Ploegh, H., and Finley, D. (2002) Multiple associated proteins regulate proteasome structure and function. *Mol. Cell* **10,** 495–507
18. Ogur, M., St. John, R., and Nagai, S. (1957) Tetrazolium overlay technique for population studies of respiration deficiency in yeast. *Science* **125,** 928–929
19. Otwinowski, Z., and Minor, W. (1997) in *Methods in Enzymology* (Carter, C. W., Jr., and Sweet, R. M., eds) Vol. 276, pp. 307–326, Academic Press, New York
20. McCoy, A. J., Grosse-Kunstleve, R. W., Adams, P. D., Winn, M. D., Storoni, L. C., and Read, R. J. (2007) Phaser crystallographic software. *J. Appl. Crystallogr.* **40,** 658–674
21. Groll, M., Ditzel, L., Löwe, J., Stock, D., Bochtler, M., Bartunik, H. D., and Huber, R. (1997) Structure of 20S proteasome from yeast at 2.4 A resolution. *Nature* **386,** 463–471
22. Emsley, P., Lohkamp, B., Scott, W. G., and Cowtan, K. (2010) Features and development of Coot. *Acta Crystallogr. D Biol. Crystallogr.* **66,** 486–501
23. Adams, P. D., Afonine, P. V., Bunkóczi, G., Chen, V. B., Davis, I. W., Echols, N., Headd, J. J., Hung, L. W., Kapral, G. J., Grosse-Kunstleve, R. W., McCoy, A. J., Moriarty, N. W., Oeffner, R., Read, R. J., Richardson, D. C., Richardson, J. S., Terwilliger, T. C., and Zwart, P. H. (2010) PHENIX: a comprehensive Python-based system for macromolecular structure solution. *Acta Crystallogr. D Biol. Crystallogr.* **66,** 213–221
24. Chen, V. B., Arendall, W. B., 3rd, Headd, J. J., Keedy, D. A., Immormino, R. M., Kapral, G. J., Murray, L. W., Richardson, J. S., and Richardson, D. C. (2010) MolProbity: all-atom structure validation for macromolecular crystallography. *Acta Crystallogr. D Biol. Crystallogr.* **66,** 12–21
25. Pettersen, E. F., Goddard, T. D., Huang, C. C., Couch, G. S., Greenblatt, D. M., Meng, E. C., and Ferrin, T. E. (2004) UCSF Chimera–a visualization system for exploratory research and analysis. *J. Comput. Chem.* **25,** 1605–1612
26. Laskowski, R. A. (2009) PDBsum new things. *Nucleic Acids Res.* **37,** D355–359
27. Rinaldi, T., Hofmann, L., Gambadoro, A., Cossard, R., Livnat-Levanon, N., Glickman, M. H., Frontali, L., and Delahodde, A. (2008) Dissection of the carboxyl-terminal domain of the proteasomal subunit Rpn11 in maintenance of mitochondrial structure and function. *Mol. Biol. Cell* **19,** 1022–1031
28. Malc, E., Dzierzbicki, P., Kaniak, A., Skoneczna, A., and Ciesla, Z. (2009) Inactivation of the 20S proteasome maturase, Ump1p, leads to the instability of mtDNA in *Saccharomyces cerevisiae*. *Mutat. Res.* **669,** 95–103
29. Lee, D. H., and Goldberg, A. L. (1998) Proteasome inhibitors: valuable new tools for cell biologists. *Trends Cell Biol.* **8,** 397–403
30. Braun, H. A., Umbreen, S., Groll, M., Kuckelkorn, U., Mlynarczuk, I., Wigand, M. E., Drung, I., Kloetzel, P. M., and Schmidt, B. (2005) Tripeptide mimetics inhibit the 20 S proteasome by covalent bonding to the active threonines. *J. Biol. Chem.* **280,** 28394–28401
31. Förster, A., Masters, E. I., Whitby, F. G., Robinson, H., and Hill, C. P. (2005) The 1.9 Å structure of a proteasome-11S activator complex and implications for proteasome-PAN/PA700 interactions. *Mol. Cell* **18,** 589–599
32. Förster, A., Whitby, F. G., and Hill, C. P. (2003) The pore of activated 20S proteasomes has an ordered 7-fold symmetric conformation. *EMBO J.* **22,** 4356–4364
33. Rabl, J., Smith, D. M., Yu, Y., Chang, S. C., Goldberg, A. L., and Cheng, Y. (2008) Mechanism of gate opening in the 20S proteasome by the proteasomal ATPases. *Mol. Cell* **30,** 360–368
34. McCutchen-Maloney, S. L., Matsuda, K., Shimbara, N., Binns, D. D., Tanaka, K., Slaughter, C. A., and DeMartino, G. N. (2000) cDNA cloning, expression, and functional characterization of PI31, a proline-rich inhibitor of the proteasome. *J. Biol. Chem.* **275,** 18557–18565
35. Bader, M., Benjamin, S., Wapinski, O. L., Smith, D. M., Goldberg, A. L., and Steller, H. (2011) A conserved F box regulatory complex controls proteasome activity in *Drosophila*. *Cell* **145,** 371–382
36. Tian, G., Park, S., Lee, M. J., Huck, B., McAllister, F., Hill, C. P., Gygi, S. P., and Finley, D. (2011) An asymmetric interface between the regulatory and core particles of the proteasome. *Nat. Struct. Mol. Biol.* **18,** 1259–1267
37. Lander, G. C., Estrin, E., Matyskiela, M. E., Bashore, C., Nogales, E., and Martin, A. (2012) Complete subunit architecture of the proteasome regulatory particle. *Nature* **482,** 186–191
38. Holm, L., and Rosenström, P. (2010) Dali server: conservation mapping in 3D. *Nucleic Acids Res.* **38,** W545–549
39. Kleijnen, M. F., Roelofs, J., Park, S., Hathaway, N. A., Glickman, M., King, R. W., and Finley, D. (2007) Stability of the proteasome can be regulated allosterically through engagement of its proteolytic active sites. *Nat. Struct. Mol. Biol.* **14,** 1180–1188
40. Osmulski, P. A., Hochstrasser, M., and Gaczynska, M. (2009) A tetrahedral transition state at the active sites of the 20S proteasome is coupled to opening of the α-ring channel. *Structure* **17,** 1137–1147
41. Larkin, M. A., Blackshields, G., Brown, N. P., Chenna, R., McGettigan, P. A., McWilliam, H., Valentin, F., Wallace, I. M., Wilm, A., Lopez, R., Thompson, J. D., Gibson, T. J., and Higgins, D. G. (2007) Clustal W and Clustal X version 2.0. *Bioinformatics* **23,** 2947–2948

SUPPLEMENTAL DATA

Structure of a Proteasome-Pba1-Pba2 Complex: Implications for Proteasome Assembly, Activation, and Biological Function

Beth M. Stadtmueller, Erik Kish-Trier, Katherine Ferrell, Charisse N. Petersen, Howard Robinson, David G. Myszka, Debra M. Eckert, Tim Formosa, Christopher P. Hill

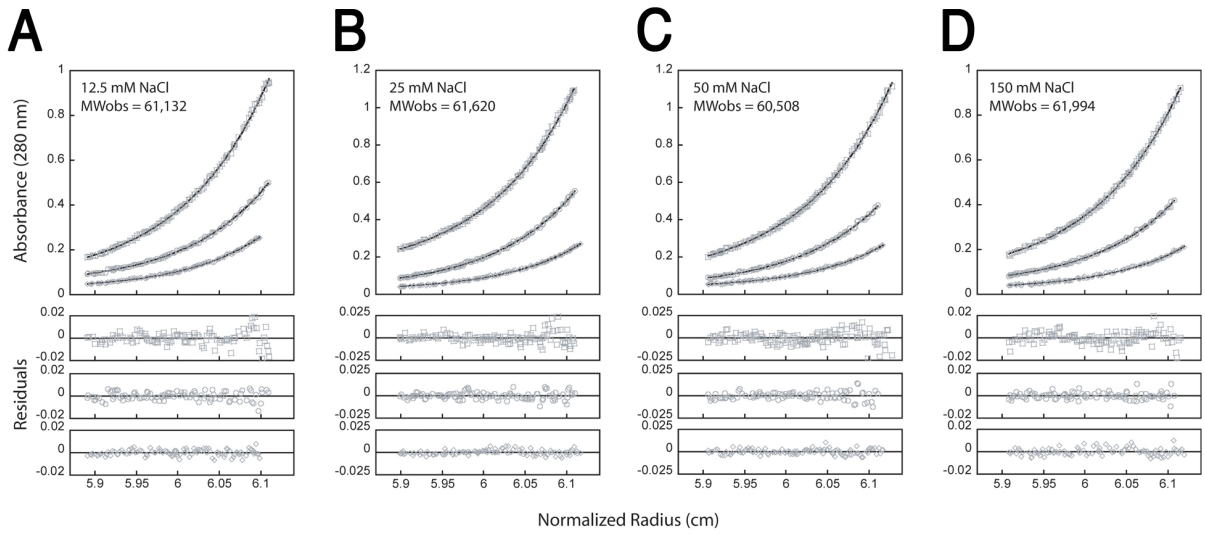

FIGURE S1. Pba1-Pba2 is a heterodimer. Analytical ultracentrifugation equilibrium sedimentation data shown here at 14,000 rpm in different salt concentrations and 20 mM Tris-HCl pH 7.5, and 2 mM TCEP. *A*, 12.5 mM NaCl. *B*, 25 mM NaCl. *C*, 50 mM NaCl. *D*, 150 mM NaCl. In all cases, the observed molecular weight (MWobs) agreed with the calculated value for a heterodimer (63,019 Da) with less than 4% error. Bottom panels show the residual differences between the data and a single ideal species fit with a floating molecular weight.

Purified His-tagged Pba1-Pba2 was dialyzed into 20 mM Tris 7.5 and 2 mM TCEP made up with 12.5, 25, 50 or 150 mM NaCl and diluted to 0.37, 0.185, or 0.0925 mg/ml. Data were collected at 4°C in an Optima XL-A centrifuge (Beckman) at 10,000 and 14,000 rpm and were globally fit to an ideal single species model with a floating molecular weight using non linear least squares analysis as implemented in HETEROANALYSIS (1). Buffer densities and protein partial specific volumes were calculated with SEDNTERP (version 1.09) (2).

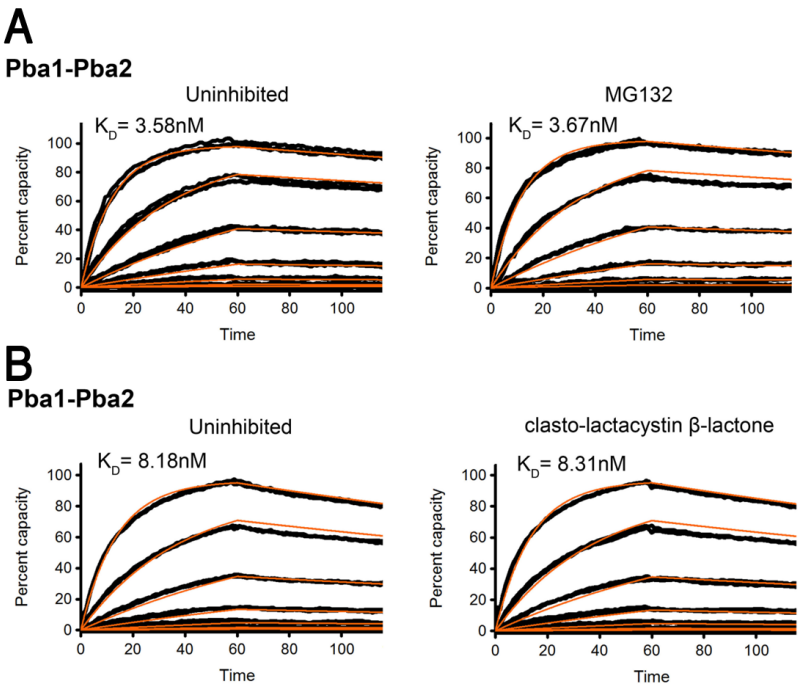

FIGURE S2. Pba1-Pba2 binding is independent of proteasome inhibition. *A*, Same as Fig. 1C, with sensorgrams, binding models and associated K_D resulting from Pba1-Pba2 interactions shown for uninhibited (left) and 10 μM MG132 inhibited (right) proteasome. *B*, Same as part *A* but using 50 μM clasto-lactacystin β-lactone-inhibited proteasome. Variation in binding constants estimated for uninhibited proteasome in these experiments and Fig. 1C presumably reflects systematic errors, such as estimating protein concentration, surface densities, and the presence/absence of DMSO, whereas these errors cancel between the side-by-side experiments of uninhibited vs inhibited proteasomes.

Pba1-Pba2 binding to inhibited 20S proteasomes utilized the same overall procedure as used for uninhibited surfaces (see Experimental Procedures). Proteasome surfaces were pre-incubated with either 10 μM MG132 in 2% DMSO or 50 μM clasto-lactacystin β-lactone for 30 minutes. MG132, which is a reversible inhibitor, was maintained in the running buffer throughout the experiment. Running buffers for control and uninhibited surfaces were supplemented with 2% DMSO for MG132-inhibited proteasomes. DMSO and inhibitor were not included in the running buffer for clasto-lactacystin β-lactone-inhibited proteasomes.

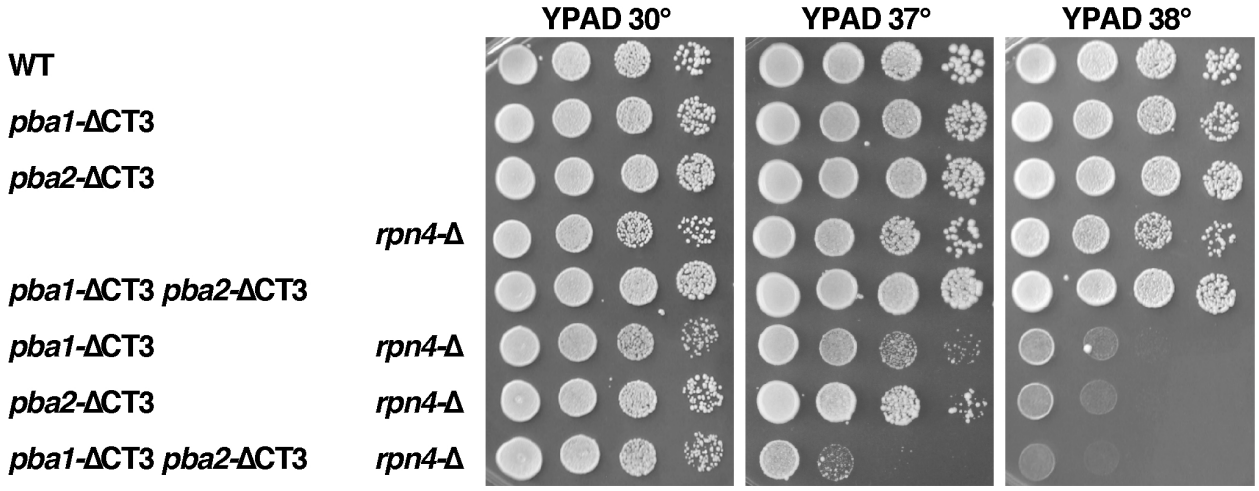

FIGURE S3. The C-terminal HbYX motifs of Pba1 and Pba2 have overlapping and unique functions *in vivo*. 10-fold serial dilutions of strains with the relevant genotypes shown (Table S2) were tested as described in Experimental Procedures in the main text. None of the single mutants caused a severe growth defect individually, but combinations of either *PBA1* or *PBA2* mutation with *rpn4-Δ* caused temperature sensitivity at 38°. These C-terminal mutations were not as severe as full deletions, as loss of growth at 37° was observed only when the *rpn4*-Δ deletion was combined simultaneously with the loss of both HbYX motifs. Complete loss of Pba1 or Pba2 proteins therefore leaves the other protein without a partner and unable to function, but loss of just one HbYX motif apparently allows the formation of a partially functional dimer, with less severe phenotypic consequences.

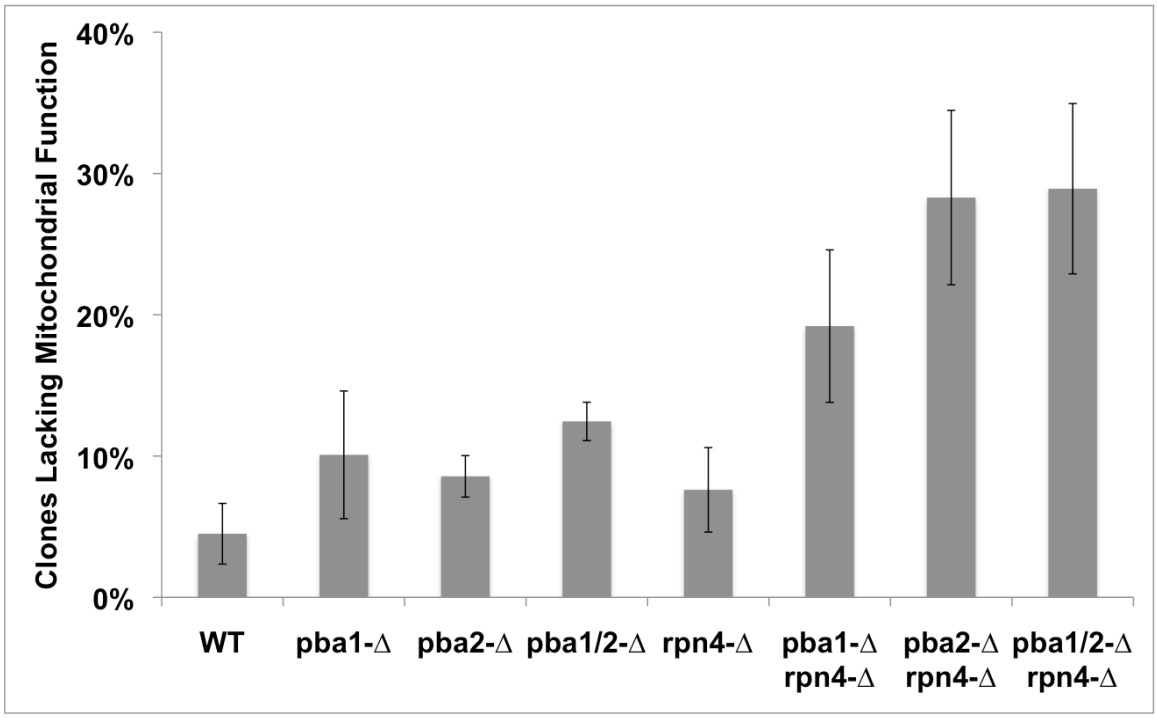

FIGURE S4. Pba1 and Pba2 contribute unique functions to the maintenance of mitochondrial activity. Isogenic strains with the relevant genotypes shown (Table S2) were grown on rich medium then tested for mitochondrial function by staining with the dye triphenyltetrazolium chloride as described (3). This assay has an inherently high variance due to the different histories of loss during growth of each culture, and this can also be affected by subtle differences among lots of media. These measurements compare a smaller number of repeats relative to the data shown in Figure 2 in the main text (3-10 independent cultures), but all were performed using a restricted set of media to limit the variance. Loss of either Pba1 or Pba2 caused a rate of mitochondrial loss similar to that observed with the *pba1-Δ pba2-Δ* double mutant, either in the presence or absence of *RPN4*, showing that each gene contributes independently to the maintenance of mitochondrial function.

	Pba1-Pba2-20S	Pba1-Pba2-20S(SeMet)	Pba1-Pba2-20S (Hg)
Data collection			
Spacegroup	$C222_1$	$C222_1$	$C222_1$
Unit cell *a,b,c* (Å)	132.4, 182.5, 388.8	132.4, 182.5, 387.8	133.8, 182.5, 386.0
Wavelength (Å)	1.075	0.9792	1.000
Resolution (Å)[a]	30-2.50 (2.59-2.50)	50-2.70 (2.80-2.70)	50-2.90 (3.00-2.90)
Rsym (%)[b]	18.2 (>100)	19.7 (87.9)	20.4 (85.1)
I/σ(I)	12.6 (2.0)	15.9 (3.4)	10.1 (2.6)
Completeness	99.8 (98.4)	100 (100)	100 (100)
Multiplicity	11.0 (8.9)	13.7 (13.6)	7.5 (7.3)
Refinement			
Resolution (Å)	30-2.50		
No. reflections	162,817		
Rwork/Rfree (%)	18.41/23.14		
No. residues	3544		
No. of waters	850		
No. of MG132	**1**		
Mean B value ($Å^2$)	27.3		
RMSD[c]			
Bond lengths (Å)	0.008		
Bond angles (°)	1.159		
Ramachandran			
Favored (%)	96.51		
Outliers (%)	0.34%		

TABLE S1. Crystallographic statistics.

Values in parenthesis refer to the highest-resolution shell.
[a] Resolution corresponds to an average I/σ(I) of at least 2.0.
[b] Although the high resolution native data R_{sym} exceeds 100%, inclusion of these data resulted in a lower R_{free}.
[c] RMSD = Root mean square deviation from ideal value.

8127-7-4	MATa ura3-Δ0 leu2-Δ0 trp1-Δ2 his3 lys2-128∂
8151-1-1	MATa ura3-Δ0 leu2-Δ0 trp1-Δ2 his7 lys2-128∂
8384-2-1	MATa ura3-Δ0 leu2-Δ0 trp1-Δ2 his7 lys2-128∂
8577-6-1	MATa ura3-Δ0 leu2-Δ0 trp1-Δ2 his7 lys2-128∂ blm10-Δ(::LEU2)
8588-N	MATa ura3-Δ0 leu2-Δ0 trp1-Δ2 his7 lys2-128∂ ump1-Δ(::NatMX)
8614-2-2	MATa ura3-Δ0 leu2-Δ0 trp1-Δ2 his7 lys2-128∂ pba1-Δ(::HphMX) pba2-Δ(::KanMX)
8634-9-1	MATa ura3-Δ0 leu2-Δ0 trp1-Δ2 his3 lys2-128∂ blm10-Δ(::LEU2)
8622-4-3	MATa ura3-Δ0 leu2-Δ0 trp1-Δ2 his3 lys2-128∂ blm10-Δ(::LEU2) pba1-Δ(::HphMX) pba2-Δ(::KanMX)
8760-6-2	MATa ura3-Δ0 leu2-Δ0 trp1-Δ2 his3 lys2-128∂ pre9-Δ(::KanMX)
8799-13-3	MATa ura3-Δ0 leu2-Δ0 trp1-Δ2 his7 lys2-128∂ pba1-Δ(::HphMX) pba2-Δ(::KanMX) rpn4-Δ(::NatMX)8801-14-1
8812-2-3	MATa ura3-Δ0 leu2-Δ0 trp1-Δ2 his3 lys2-128∂ pba1-Δ(::HphMX) pba2-Δ(::NatMX)
8812-6-2	MATa ura3-Δ0 leu2-Δ0 trp1-Δ2 his3 lys2-128∂ pba1-Δ(::HphMX) pba2-Δ(::NatMX) pre9-Δ(::KanMX)
8873-2-3	MATa ura3-Δ0 leu2-Δ0 trp1-Δ2 his7 lys2-128∂ rpn4-Δ(::KanMX)
8912-2-2	MATa ura3-Δ0 leu2-Δ0 trp1-Δ2 his7 lys2-128∂ pba1-ΔCT3(LEU2) pba2-ΔCT3(URA3)
8912-3-3	MATa ura3-Δ0 leu2-Δ0 trp1-Δ2 his7 lys2-128∂ pba1-ΔCT3(LEU2) pba2-ΔCT3(URA3) rpn4-Δ(::KanMX)
8913-4-4	MATa ura3-Δ0 leu2-Δ0 trp1-Δ2 his7 lys2-128∂ pba1-Y275A(LEU2) pba2-Y266A(URA3)
8924-2-4	MATa ura3-Δ0 leu2-Δ0 trp1-Δ2 his7 lys2-128∂ pba1-Y275A(LEU2) pba2-Y266A(URA3) rpn4-Δ(::KanMX)
8925-3-3	MATa ura3-Δ0 leu2-Δ0 trp1-Δ2 his7 lys2-128∂ blm10-Δ(::LEU2) pba1-Δ(::HphMX) pba2-Δ(::KanMX)

TABLE S2. Yeast strains used.

REFERENCES

1. Cole, J. L. (2004) *Methods Enzymol* **384**, 212-232
2. Laue, T., Shah, B., Ridgeway, T., and Pelletier, S. (1992) Computer-aided interpretation of analytical sedimentation data for proteins. Royal Society of Chemistry. pp 90–125
3. Ogur, M., St. John, R., and Nagai, S. (1957) *Science* **125**, 928-929